

Response of Ocean Surface Waves to the Co-occurrence of Boreal Summer Intra-Seasonal Oscillation and El Niño Southern Oscillation

Duphrin Joseph, Sanil Kumar V*

Ocean Engineering Division,
CSIR-National Institute of Oceanography
(Council of Scientific & Industrial Research),
Dona Paula 403 004, Goa, India
*corresponding author (sanil@nio.org)

Abstract

Studies related to the combined effect of different atmospheric oscillations on the ocean surface waves are limited. The present study focuses on the change in wave climatology due to the combined effect of Boreal Summer Intra-Seasonal Oscillation (BSISO) and El Niño Southern Oscillation (ENSO) using 40 years of reanalysis data on the Asian Summer Monsoon Region (ASMR). Composite analysis of surface wind, significant wave height, wind-sea, swell and mean wave period are analysed corresponding to different ENSO-BSISO phase combinations. The study showed noteworthy differences in wave parameters when ENSO-BSISO phases are analysed together. In El Niño-BSISO combined phase, enhancement of north-easterly wind causes the advancement in the reversal of wind direction (north-easterly to monsoon enhanced south-westerly) and disrupted propagation of positive wind and wave anomalies. Conversely, during La Niña-BSISO co-occurrence, south-westerlies are enhanced and as a result, the negative north-easterly anomalies are disrupted. In all the ENSO-BSISO combined phases, maximum wave height variability occurs at the South China Sea owing to the combined action of the north Indian Ocean (NIO) and Western North Pacific (WNP) surface wind forcing. High fluctuations in T_m over the NIO and WNP are observed during different ENSO-BSISO phase combinations. The phase relationship of H_s with T_m and the significant height of wind-sea (H_{sw}) and swell (H_{ss}) are assessed to understand the propagation of swells. Due to the effect of multiple atmospheric perturbations, significant changes in H_s occur over the coastal regions of the NIO.

Keywords: Boreal Summer Intra-Seasonal Oscillation (BSISO), El Niño Southern Oscillation (ENSO), North Indian Ocean, South China Sea, Significant Wave Height, Mean Wave Period.

1 Introduction

Understanding the change in wave climate related to the fluctuations in the atmospheric circulation is important to reduce the impact of related issues such as coastal erosion and flooding. Because of the advancement in science and technology over the years, monitoring techniques for the large-scale atmospheric forcing and studies of its effect on the ocean surface are remarkably improved. A comprehensive examination of small to largescale fluctuations in the ocean surface waves is necessary for the fields of navigation, food, energy harnessing, defensive activities, etc. Since the Asian Summer Monsoon (SM) is the largest monsoon system on earth, it has a paramount effect on surface waves in the Indian Ocean (IO). The presence of complex wind systems such as Low-Level Jet (LLJ) and Findlater Jet (Findlater 1969), have a direct impact on the waves in the north Indian Ocean (NIO). During SM, the seasonal average significant wave heights (H_s) are highest (3.0-3.5 m) in NIO, and wind-sea and swell heights are peaked in western NIO because of strong Findlater jet (Anoop et al. 2015). Intensified winds and waves in the Bay of Bengal (BoB) (Glejin et al. 2013; Shanas and Kumar 2015) and Arabian Sea (AS) (Amrutha and Sanil Kumar 2017) are present during SM. Northern BoB is an area in which higher wave heights and dominance of swells are observed during SM (Sanil Kumar and Anoop 2015). In the AS, the wind-wave coupling is strong which leads to wave periods rarely above 15 s (Amrutha and Sanil Kumar 2017) and wave heights higher than 4.0 m is observed several times (Sanil Kumar and George 2016, Amrutha et. al 2019).

The summer in the South China Sea (SCS) is characterised by low wave intensity compared to other seasons due to relatively low wind speeds (Su et al. 2017). Since the SCS is a semi-enclosed region, locally generated wind-seas dominate over the swells in the SCS in summer when the winds are strong. On the other hand, in the spring season, where the local winds are weakest of the year, the H_s variations in SCS are significantly influenced by the swells (Su et al. 2017). The swells generated due to winds in the Western North Pacific (WNP) influence the waves in SCS more than the swells due to winds in NIO. Earlier studies (Mirzaei et al. 2013, Han et al. 2017) reported the increase in H_s due to El Niño in SCS. The WNP region is more affected by the El Niño Southern Oscillation (ENSO) due to the high convective activity. Shimura et al. (2015) observed that the summertime H_s in WNP is mostly affected by tropical cyclone (TC) and ENSO events due to the rapid changes in Sea Surface Temperature (SST). The swell propagating from the Northern Pacific and the Southern Ocean (SO) also affects the wave climate of WNP (Jiang and Chen 2013). Hence, the atmospheric oscillations associated with SM have crucial impacts on the wave climate of the NIO and WNP.

Intra-seasonal oscillations during SM have a great impact on the wave climate in the NIO and WNP (Li Chong-Yin and Zhou Ya-Ping 1994). The impact of individual atmospheric oscillations on surface waves is addressed in earlier studies. Boreal Summer Intra-Seasonal Oscillation (BSISO) dominates in the Asian Summer Monsoon Region (ASMR) during June-October (Madden and Julian 1972; Krishnamurti and Subrahmanyam 1982). BSISO is dominated by strong northward propagation of 30-60 days in the IO and north-westward propagation of 10-20 days in the western Pacific (WP) and these two propagations are independent (Yasunari 1979; Jiang et al. 2004). The life cycle of BSISO falls into eight distinct phases. Each phase represents convection over different regions (Hsu et al. 2017). Kikuchi et al. (2012) give the phase space representation for BSISO in detail. The first phase starts from the Equatorial IO (EIO) followed by north-eastward propagation towards BoB in phases 2 and 3. In phases 4 and 5 the convection activity is over the Indian and Maritime continent. Further, it moves eastward to WNP in phases 6 and 7. Finally, reaches the EIO in phase 8 and completes the phase cycle (Hsu et al. 2017). Recently, Srinivas et al. (2020) noted negative H_s anomalies in NIO during phases 1 to 3 of BSISO in response to the easterly wind anomalies and high positive H_s anomalies during phases 5 to 7 in response to the westerly wind anomalies over the NIO.

Effects of ENSO on the ocean surface waves were analysed recently by many researchers (Kumar et al. 2019; Odériz et al. 2020; Patra et al. 2020; Shanas et al., 2017). Lin (2019) noticed that convection (precipitation) occurs in the eastern EIO and Maritime continents (the subtropical SCS and WP) after El Niño (La Niña). The disturbance in Walker circulation during ENSO teleconnection leads to dispersion of baroclinic equatorial atmospheric waves causing an overall change in atmospheric circulation in tropical areas (Lin et al. 2007). In the EOF2 mode of BSISO, Li and Mao (2019) found enhanced (weakened) activity over the south-eastern equatorial IO (equatorial WP) in the La Niña developing summers and vice versa in El Niño developing summers. These kinds of atmospheric activities can be altered when it co-occurs with another atmospheric perturbation such as BSISO. Many researchers found that BSISO has significant changes due to the co-occurrence with ENSO (Yun et al. 2008; Liu et al. 2016; Lin 2019; Chen et al. 2020). Pillai and Chowdary (2016) stated that the 30-60 day BSISO has strongly modulated than 10-20 day oscillation because of the changes in the seasonal mean state associated with El Niño. El Niño occurrence can cause the abnormal enhancement of Intra-Seasonal Oscillations (ISO). The important influences of ENSO are also obvious to the ISO in the tropical atmosphere. During El Niño, ISO is reduced and changes the barotropic structure in the tropical atmosphere (Li Chong-Yin and Zhou Ya-Ping 1994).

The studies on wave conditions related to the co-occurrence of multiple atmospheric oscillations are limited (eg., Kumar et al. 2016; Godoi et al. 2019; Patra et al. 2020; Remya et al. 2020). These studies revealed strong changes in wave conditions when multiple oscillations combine. For instance, Remya et al. (2020) identified reduced swell generation from the Southern Ocean (SO) and increased swell generation from the Eastern Tropical IO when Southern Annular Mode (SAM) and La Niña co-occur. Similarly, Kumar et al. (2016) revealed a stronger (weaker) influence on extreme wave heights when the same (opposite) phases of ENSO and Pacific Decadal Oscillation (PDO) co-occur. The above studies reveal the urgency to assess wave conditions during the conjunction of multiple oscillations. The influence of the co-occurrence of BSISO with ENSO on the surface waves is not explored so far. Hence, the present study aims to analyse the changes in wave parameters during the co-occurrence of the BSISO and ENSO.

The paper is organized as the following: Section 2 describes the data and methods used in this study. In section 3, the obtained results are described and discussed. Section 4 presents the conclusions of the study.

2 Data and Methodology

We used 40 years of daily reanalysis data of 10 m zonal and meridional wind (u , v), significant height of combined wind-seas and swells (H_s), significant height of swells (H_{ss}), significant height of wind-seas (H_{sw}), mean wave period (T_m) and normalized energy flux into waves (E_{fw}). All these datasets were obtained from the European Centre for Medium-Range Weather Forecasts (ECMWF) reanalysis v5 (ERA5) with a resolution of $0.5^\circ \times 0.5^\circ$ for the period 1979 to 2018 (Hersbach et al. 2020). The previous study by Naseef and Sanil Kumar (2020) reported ERA5 H_s show a good agreement with measured buoy data in the coastal (bias ~ 0.29 m) and deep waters (bias ~ 0.18 m) of NIO. Besides, few have validated ERA5 surface wind data with in situ observations and satellite observations and applied it in long-term wave climate studies (Ramon et al. 2019; Aboobacker et al. 2020). E_{fw} is the normalised vertical flux of energy from the wind into the ocean waves. A positive flux implies a flux into the waves. The unit of E_{fw} is W/m^2 , it is normalised by dividing by the product of air density and the cube of the friction velocity.

The daily BSISO index data were obtained from the Asia-Pacific Data-Research Center (APDRC) of the International Pacific Research Center (IPRC). The BSISO modes are calculated with the extended empirical orthogonal function (EEOF) analysis for June-July-August-September (JJAS) period. The intra-seasonal variability was extracted by applying Lanczos band-pass filter (Duchon 1979) with cut-off periods 25 and 90 days and 141 weights to the daily Outgoing Longwave

Radiation (OLR) data before performing the EEOF analysis (Kikuchi et al. 2012). Oceanic Nino Index (ONI) was taken from the NOAA Climate Prediction Center. ONI values are defined by 3 months running mean of SST anomalies in the NINO 3.4 region.

In this study, we followed the method used by Godoi et al. (2020) to find the combination of ENSO-BSISO co-occurring phases. Days with strong ENSO and BSISO activities were identified to assess the wave conditions during the peak atmospheric oscillations. Strong ENSO events were identified when the ONI value remained above 0.5 (El Niño) or below -0.5 (La Niña) for 5 consecutive seasons and the rest is considered as neutral ENSO. In order to convert the monthly index to daily, the value of each month was assigned to every day of that month. The strong BSISO activity was identified by setting the threshold value of 1.5 to the BSISO index.

Composite analysis corresponding to the 3 phases of ENSO and 8 phases of BSISO co-occurring days corresponding to the summer monsoon period (JJAS) was carried out. The domain selected for composite analysis was from 40°E-160°E and 10°S–30°N, which is the region through the BSISO propagation is most prominent. The total number of days in which ENSO phases co-occurs with BSISO phases during the period 1979 to 2018 is given in Table 1. These are the days upon which composite analysis of anomalies of wind speed (W_s), H_s , H_{sw} , H_{ss} , T_m was carried out. The results are important in closely analysing the teleconnection of ENSO and BSISO induced atmospheric disturbances to the ASMR. The disturbance in Walker circulation is the reason for these teleconnections which occur as a consequence of the change in heat and humidity in tropical oceans (Grimm and Ambrizzi 2009). These teleconnections related to ENSO cause changes in wind speed and direction thereby inducing variations in wave climate (Schott et al. 2009) in the IO. Therefore, we analysed the change in ocean surface waves due to the atmospheric forcing of combined ENSO-BSISO activity.

3 Results and discussion

Since ENSO being the most important interannual climate variability, the associated change in the Walker circulation influences the IO (Klein et al. 1999) causing regional changes in the SST and wind speeds. The change in wind anomalies thereby generates a change in the wave conditions (Schott et al. 2009). In the following section, we analyse the modifications in wave climate when the interannual oscillations co-occur with the intra-seasonal oscillations. The results and the discussions are written here in 3 sections corresponding to each ENSO phase.

3.1 Co-occurrence of Neutral ENSO with BSISO

The neutral ENSO phase with the BSISO indicates the wave anomalies controlled by the strong BSISO related wind activity (Figs. 1 and 2). The wave patterns are similar to Srinivas et al. (2020) with some notable changes in the intensity of the composites of T_m and H_s in BoB and AS (Fig. 2). During phase 1, strong negative north-easterly wind anomaly close to 4 m/s (Fig. 1 a) dominate all over the NIO, whereas a positive anomaly is prominent over the maritime continent and WNP. This negative anomaly shows strong northward and weak eastward propagation in the NIO and WNP as a response to BSISO up to phase 4 (Fig 1 a-d). The eastward propagation is very weak in the WNP. From the 4th phase onwards south-westerly wind starts to appear in the lower part of NIO as a response to the SM wind system. From phases 5 to 7, positive south-westerly wind anomaly (~ 2.5 m/s) follows the BSISO propagation pattern (Fig. 1 e-g). Phase 8 represents the transition from south-westerlies to north-easterlies in the AS. In phase 8, strong negative north-easterly wind anomalies (~ -3.5 m/s) are present in the AS, whereas south-westerly wind anomalies are present over the rest of the NIO. Wind activity is very strong (wind anomaly ~ 4 m/s) because of converging south-westerly and north-easterly winds in the SCS in phase 8 (Fig. 1 h) and this positive anomaly continues to prevail in phase 1 with weak anomalies in SCS (Fig. 1 a). AS shows a faster response to the shift in wind system from north easterlies to south westerlies compared to the WNP.

The H_s anomaly follows a similar pattern to the wind. Strong negative H_s (~ -0.6 m in phase 1 over AS) anomalies propagate northwards in the NIO with reducing intensity (~ -0.1 m in phase 4 over AS) over phases 1 to 4 (Fig. 2 a-d). While in the WNP and SCS, negative anomalies prevail up to phase 5 (Fig. 2 a-e). WNP shows minimum eastward propagation. Positive anomalies of H_s due to the action of BSISO south-westerly wind anomalies on the mean SM south-westerly wind from phase 5 to phase 8 (Fig. 1 e-h), also show a similar propagation pattern as in the first 4 phases. High H_s anomaly ~ 0.7 m is seen over the western Indian, Bangladesh and Myanmar coasts in phase 6 (Fig. 2 f). In SCS maximum H_s anomaly (~ 0.7 m) was observed at the Philippine islands during phase 7 (Fig. 2 g). The reduced (increased) energy flux into the waves from the wind shows good agreement with the H_s anomalies from phases 1 to 4 (5 to 8) over NIO.

Interpreting the T_m is a good method to understand whether the area is dominated by wind-seas or swells. Kumar et al (2000) and Aboobacker et al. (2011) observed higher wind-seas and swells in the coastal regions of eastern AS during SM, indicating a mixed sea state. The 40° - 60° S band of the SO (Sabique et al. 2012) and 20° S band (Remya et al. 2020) are the two important swell generating area in the IO. Long-period waves from the SO reaches the west coast of India quite frequently (Amrutha et al. 2017). The swells from the SO propagate more towards the BoB and

Maritime continent during JJA (Zheng et al. 2018). The influence of SM winds causes a drop in the swell dominance on the local wave climate of the AS than the BoB due to the strong and persistent wind (Sabique et al. 2012). Amores and Marcos (2020) identified swell generating area in WNP and tracked the swell events, which reaches the Philippine Islands. Similarly, the swell propagating from the SO also reaches the WNP (Jiang and Chen 2013; Li 2016). These observations set the explanations for the swell activities in the NIO and WNP. The T_m anomaly shows notable changes from Srinivas et al. (2020). For example, they obtained an in-phase relationship with H_s and T_m in AS, WNP and out of phase relation in BoB in all the phases. But when only the peak BSISO days are considered, we observed out of phase relation in AS, BoB and WNP but in-phase relation in SCS. The southern AS and BoB experiences swell propagation from the SIO, while the WNP experiences swell from NP and SO. The strong negative (positive) wind anomaly in these regions leads to the decreased (increased) energy flux into the higher frequencies and as a result, T_m increases (decreases). This explains the reason for out of phase relationship between wind anomaly and T_m . Phases 1 to 5 in the AS and BoB are dominated by negative wind anomaly, hence positive T_m anomaly (Fig. 1 a-e). This happens vice versa in phases 6 and 7 (Fig. 1 f-g). In the first phase (Fig. 2 i) waves with higher T_m anomaly ($\sim 2s$) occur in the south-eastern AS and south-western BoB and shift northward in phase 2 (Fig. 2 j). Whereas, Srinivas et al. (2020) reported strong negative T_m anomalies in phases 1 and 2 over AS. This indicates the intensified BSISO reduces the wind, which in turn reduces short-period wave propagation in phases 1 and 2. The swell propagation from the tropical IO due to the action of easterly winds (Remya et al. 2020) enhances the T_m in phases 1 and 2. From phase 5 to phase 8, positive T_m anomalies are noticed over the maritime continent and WNP. To understand the phase relationship of T_m with H_s we studied H_{sw} and H_{ss} in detail.

Both H_{sw} and H_{ss} show negative anomaly from phases 1 to 4 (Fig. 3 a-d & i-l) in AS, BoB and WNP, while phases 5-7 (Fig. 3 e-g & m-o) show positive anomaly due to the increase in south-westerly wind. This further support the explanation for out of phase relationship in these areas. An increase (decrease) in wind in the SCS leads to an increase (decrease) in both H_{sw} and H_{ss} indicating the region is dominated by locally generated winds. This explains the in phase relationship of wind and T_m in SCS. Maximum H_{sw} (0.9 m) and H_{ss} (1 m) anomalies are seen over the SCS in phase 8 due to the strong south-westerlies. Overall, the BSISO has a significant impact on waves by regulating the wind.

3.2 Co-occurrence of El Niño with BSISO

The negative north-easterly wind anomaly which was predominant over the AS and BoB in phases 1 and 2 during individual BSISO occurrence weakens remarkably and starts to turn to south-

westerlies when El Niño combines with BSISO (Fig.4 a-b). At the same time, the south-westerly wind that prevails over the SCS and WNP gets intensified (anomaly $\sim 3\text{m/s}$) in phase 1 and is rapidly replaced by easterly winds from the equatorial Pacific Ocean (EPO). The El Niño enhances the south-westerly winds from phases 1 to 4 causing the faster diminishing of mean north-easterlies in NIO. In phase 3, a strong south-westerly wind anomaly of $\sim 3.5\text{ m/s}$ is identified over the central and southern BoB (Fig.4 c), which further intensified ($\sim 4\text{m/s}$) and shifted to the southern tip of India in phase 4 (Fig.4 d). Meanwhile, north-easterly wind from the northern EPO in phase 2 propagates to the WNP. A significant intensification of north-easterlies can be seen over the WNP due to the effect of El Niño-BSISO co-occurrence from phases 2 to 4 (Fig. 4 b-d). This intensification peaks ($\sim 4\text{ m/s}$) in phase 4 over the Philippine region (Fig. 4 d). During SM, easterlies are stronger than usual in the western EPO due to the shifting of the South Pacific Convergence Zone (SPCZ) (Rasmusson and Carpenter 1982). From phases 5 to 7 the El Niño related north-easterly wind is enhanced and it causes a decline of mean south-westerlies in the NIO. The diminished westerly wind anomaly in the NIO (anomalies $< 1.5\text{ m/s}$) propagates to the north-east towards the Pacific, while it gets intensified in the SCS and western EPO (Fig. 4 e-g). The winds in the IO rapidly decrease in phases 5 and 6 (Fig. 4 e-f). From phase 7 onwards the transition to easterlies starts in the southern AS (Fig. 4 g). This implies that the effect of El Niño-BSISO co-occurrence causes a reversal in wind direction (north-easterlies to south-westerlies) earlier than during the independent BSISO occurrence.

The changes in wind patterns are seen in the anomalies and propagation of wave parameters. In phase 1, a strong core of negative H_s anomaly ($>1\text{ m}$) is seen over the AS, which enlarged and intensified in phase 2 (Fig. 5 a-b). From phase 2 to 4 (Fig.5 b-d) negative anomaly showed a weak eastward propagation than the neutral ENSO-BSISO phase. In phase 4, a strong positive H_s anomaly is seen at the tip of India due to the wind intensification (Fig. 5 d). Positive H_s anomalies start to show up early in the AS and BoB due to the effect of El Niño in phase 5 (Fig. 5 e) and prevail all over the NIO, SCS and maritime continent by phase 6 (Fig. 5 f). Maximum H_s anomaly (1 m) occurs at the Sri Lankan coast in phase 4. The H_s in the AS is less than that in the BoB in these phases. Kumar et al. (2019) also observed that H_s is relatively low during El Niño years in the AS. Negative anomalies start to appear in the AS in phase 7, which intensifies and shifts northward from phase 8 (Fig. 5h). Maximum H_s is seen in the SCS along Vietnam and south-east China coast in phase 6 even though the winds are weak, which reveals the swell dominance in the SCS. Many researchers have noted disagreement between wind and H_s conditions due to the dominance of swell in the SCS (Chu et al. 2004; Su et al. 2017). From all these earlier studies and our observations, SCS can be considered as a hotspot during ENSO-BSISO combined activity. The maximum value of H_s ($> 1\text{m}$)

is observed in the SCS in phase 6 (Fig. 5 f) due to the intensified south-westerlies in that region catalyzed by the combined El Niño-BSISO effect.

The T_m anomaly during El Niño displayed significant variation from the neutral ENSO phase. Strong positive anomalies observed during neutral ENSO-BSISO phases 1 and 2 over AS and southern BoB (Fig. 2 i-j) are absent during El Niño-BSISO co-occurrence (Fig. 5 i-j) because of the reduction in north-easterly wind anomaly. Instead, negative T_m anomalies (~ 1.5 m) are visible over the AS and central equatorial IO in phase 2 (Fig. 5 j) due to the effect of El Niño on BSISO. The T_m shows a negative anomaly in AS, BoB and WNP in the first 4 phases. The reason for this negative anomaly in the AS and BoB is that the reduced negative north-easterly wind anomalies in the 2nd phase (Fig 5 j) and the positive south-westerly anomalies in the 3 and 4 phases (Fig 5 k-l), supplies more energy to the higher frequencies. While in the WNP, the energy to the higher frequencies is supplied by the positive north-easterly anomaly in the first 4 phases (Fig 5 i-l). From phase 5 to 7 the reduction in positive south-westerly anomaly reduces the T_m by reducing the swell propagation towards AS and BoB. Strong positive T_m anomaly in the AS and BoB observed in the 1st and 2nd phases of neutral ENSO-BSISO (Fig 2 i & j) condition is only visible in phase 8 of El Niño-BSISO condition in the south-eastern AS and southern BoB (Fig. 5 p). This is due to the negative energy flux into the waves in all these phases (Fig. 1 i-j & Fig. 4 p). Overall the out of phase relationship between the wind and T_m anomaly is visible on the AS, BoB and WNP, yet it is weak compared to the neutral ENSO-BSISO phase due to the lower swell domination by the reduced wind. In the SCS, it shows in phase relationship with the wind anomaly and overall T_m positive anomaly is reduced due to the reduction in the south-westerly wind.

The pattern of energy flux into the waves is more complex in El Niño-BSISO co-occurring time (Fig. 4 i-p). A slight positive anomaly in energy flux in the northern AS, in phases 1 and 2 (Fig. 4 i-j), leads to positive H_{sw} (Fig. 6 a-b) and reduced H_{ss} (Fig. 6 i-j). The maximum energy flux is seen in phases 3 and 4 in the southern BoB and southern tip of India (Fig. 4 k-l) enhances the wind-seas and thereby H_{sw} (Fig. 6 c-d).

Both the H_{ss} and H_{sw} in the AS exhibit a significant reduction in AS and BoB compared to the neutral ENSO-BSISO phase due to the reduction in south-westerlies. Phases 1 to 4 are characterized by negative H_{ss} and H_{sw} anomaly in AS and northern BoB (Fig. 6 a-d & i-l) due to the negative north-easterly wind anomalies, whereas phase 5 and 6 shows a positive anomaly in both (Fig. 6 e-f & m-n) due to the positive south-westerly wind anomalies. Amrutha et al. (2015) observed that intermediate period waves with peak wave periods between 6s and 12 s dominate the central west coast of India. Also, earlier studies (Kumar et al. 2000; Aboobacker et al. 2011) observed that the

direction of swell in the eastern Arabian Sea is south-west. Hence, due to the drop in south-westerly winds, the northern and north-western AS shows negative H_{ss} in all the phases. The lower south-westerlies reduce the deflection of swell propagation towards the north-west direction and more swell propagates towards the east. Hence, the swell height is positive in the Maritime continent and southern BoB in phases 4 to 7 (Fig 6 l-p).

3.3 Co-occurrence of La Niña with BSISO

Fig. 7 explains the change in wind speed and direction in the peak La Niña-BSISO co-occurring days. The effect of La Niña enhances the south-westerly wind in NIO. As a result, a notable decrease in the negative anomaly in north-easterly winds compared to the neutral ENSO-BSISO phase at NIO occurs in the first 4 phases (Fig. 7 a-d). In the WNP, weak easterly winds followed by phase 1 are intensified in phase 2 (Fig. 7 a-b). This strong easterly wind is due to the flow from the eastern Pacific to the low pressure over the WP during La Niña as a response to the high SST anomalies. In 2nd phase, the easterly winds are with higher speed (>3.5 m/s) over the WNP. From phase 3 onwards the south-westerlies start to prevail in the southern AS. From phases 5 to 8 south-westerlies prevail with strong northward and weak eastward propagation as seen in the neutral ENSO condition (Fig. 7 e-f). Interestingly, the south-westerlies continue to prevail in phases 1 and 2 with a low intensity over the NIO due to the enhancement of wind. Hence, the effect of La Niña delays the effect of BSISO north-easterly winds in both the NIO and WNP.

The H_s anomaly is weakened in La Niña-BSISO phase 1 to 5 (Fig. 8 a-e). The negative H_s anomaly due to north-easterlies starts to dominate only in phase 2 in the AS, BoB and SCS (Fig.8 b). In phase 1 a strong positive H_s anomaly (~ 4 m) is seen in the ECS (Fig.8 a) due to the intensified wind (Fig.7 a). In phase 3, the negative anomaly from the AS and BoB shift to the east and gets intensified in the SCS and WNP in phase 4 (Fig. 8 c-d), while the positive anomaly starts to propagate in the northeast direction in the AS and BoB. Positive H_s anomaly picks up over the NIO at a slower pace than neutral ENSO-BSISO time due to the suppressed winds in phases 3 and 4 (Fig. 7 c-d). Positive H_s shows fast north-eastward propagation than neutral ENSO conditions. Positive H_s anomaly is highly intensified (>1 m) in the SCS in phase 7 (Fig. 8 g). The SCS showed a high H_s anomaly during La Niña-BSISO time in phase 8 (Fig. 8 h) than the neutral-ENSO condition (Fig. 2 h) due to the reduced action of north-easterly winds on the south-westerlies.

Strong positive T_m anomalies in phases 1, 2, and 8 during the Neutral ENSO-BSISO phase (Fig. 2 i, j & p) were replaced by negative anomalies during La Niña-BSISO phase (Fig. 8 i,j & p) due to the abatement in negative wind anomaly. Similar to the neutral ENSO-BSISO, the out of

phase relation between wind and T_m is present in the AS, BoB and WNP and in phase relation in the SCS. From phase 3 to 7, a positive T_m anomaly is present in the maritime continent and eastern equatorial IO (Fig. 8 k-o). This can be due to high period wave propagation because of the intensified south-westerly wind. Maximum T_m anomaly (>2 s) occurs in the ECS in phase 2 on the account of strong wind activity (Fig. 8 j).

The suppressed wind over the NIO during La Niña is evident on the E_{fw} . The strong negative E_{fw} anomaly occurred during the Neutral ENSO-BSISO phases 1 to 3 (Fig.1 i-k) diminished in the La Niña-BSISO phase (Fig.7 i-k). The maximum E_{fw} occurs in the WNP in phase 2 due to the increased convective activity and easterly wind because of La Niña (Fig.7 j). High wind flux in the SCS during phase 6 to phase 8 (Fig.7 n-p) implies the increased H_s over that region (Fig.8 f-h).

In general, both H_{ss} and H_{sw} are enhanced in the La Niña-BSISO phase than the other two ENSO and BSISO co-occurring phases. Similar to the wind pattern, negative anomalies of both H_{ss} and H_{sw} get weakened during La Niña in phases 1 to 4 (Fig.9 a-d & i-l). From phase 5 to 7, strong south-westerly generated wind-seas and swell are present over the AS and BoB (Fig. 9 m-o). The WNP shows an overall reduction in swell than the neutral ENSO- BSISO phase due to the reduced generation of wind-seas and swells in the NP due to the decreased wind.

4 Conclusions

The BSISO independent occurrence is characterised by negative north-easterly anomalies from phase 1 to 4 and positive south-westerly anomalies from phase 5 to 8. Both these anomalies follow a north-eastward propagation pattern as a response to BSISO. When BSISO combines with El Niño, the north-easterly wind is enhanced. On the other hand, the south-westerly wind is enhanced when it combines with La Niña. The effect of El Niño-BSISO co-occurrence causes a reversal in wind direction (north-easterlies to south-westerlies and vice versa) earlier than independent BSISO occurrence. La Niña-BSISO combined activity strengthens the easterlies in the WNP due to the convection over the maritime continent and suppresses the easterlies in the NIO.

Due to the change in the surface wind, during El Niño-BSISO (La Niña-BSISO) co-occurrence, the negative (positive) anomalies of W_s and H_s shows more intact north-eastward propagation during phase 1 to 4 (phase 5 to 8) while the propagation of positive (negative) anomalies are disrupted. The ENSO makes a prominent variation in H_s when co-occurring with BSISO. The maximum positive anomaly of H_s is observed in the EIO, southern tip of India, maritime continent and the coastal regions of Philippines and Vietnam during El Niño-BSISO co-occurrence. While the La Niña-BSISO combined activity increases H_s in the central-western and north-eastern coast of

India and western coast of Bangladesh during phase 6. These increasing wave heights are important since the anomalous increase in wave height can escalate the wave power and thereby can cause erosion and coastal flooding.

T_m shows an out of phase relationship with the wind in AS, BoB and WNP, which indicates the dominance of swell over these regions. The in-phase relationship between H_s and T_m in the SCS in all the ENSO-BSISO phases indicates that wind-activated wind-seas and swells dominate SCS. H_{ss} and H_{sw} are maximum in the SCS during the El Niño-BSISO phase. Swell height is high over the BoB, maritime continent, WNP from phases 5 to 8 in all ENSO conditions highlighting the propagation of SIO swells to that region.

The SCS is a very dynamic region due to the action of surface forcing from both the IO and WNP. Rapid changes in the wind system lead to the sudden change in wave parameters in the SCS. Being a semi-enclosed sea, the maximum and minimum peaks of H_s anomalies that occur in the SCS makes the coastal region around it highly vulnerable to the resulting effects.

The difference in the values of wave parameters observed during BSISO independent activity and the ENSO-BSISO combined activity indicates the need for studies on the impact of the combination of different atmospheric oscillations on the ocean surface waves. Since both intra-seasonal and inter-annual oscillations individually cause significant changes in wave climate, the combined action of these two can cause pronounced changes and this needs to be assessed.

Acknowledgements

ERA5 data used in this study are downloaded from the ECMWF data server: <http://data.ecmwf.int/data>. The authors acknowledge the Council of Scientific and Industrial Research, New Delhi for funding the research work. The authors thank Aravind P, Jesbin George and Shanas P R for the constant support during the study. The authors wish to acknowledge the use of Python, Matlab and Ferret for analysis and graphics in this paper. The authors thank the reviewers for the comments and suggestions, which improved the content of the paper. This publication is CSIR-NIO contribution ----- and forms part of the proposed Ph.D. work of the first author.

References

- Aboobacker VM, Rashmi R, Vethamony P, Menon HB (2011) On the dominance of pre-existing swells over wind seas along the west coast of India. *Cont Shelf Res* 31:1701–1712. <https://doi.org/10.1016/j.csr.2011.07.010>
- Aboobacker VM, Shanas PR, Al-Ansari EMAS, et al (2020) The maxima in northerly wind speeds and wave heights over the Arabian Sea, the Arabian/Persian Gulf and the Red Sea derived from 40 years of ERA5 data. *Clim Dyn*. <https://doi.org/10.1007/s00382-020-05518-6>
- Amrutha MM, Sanil Kumar V (2017) Characteristics of high monsoon wind-waves observed at multiple stations in the eastern Arabian Sea. *Ocean Sci Discuss*. <https://doi.org/10.5194/os-2017-84>
- Amrutha MM, Kumar VS, George J (2017) Observations of long-period waves in the nearshore waters of central west coast of India during the fall inter-monsoon period. *Ocean Eng*. 131, 244–262. <https://doi.org/10.1016/j.oceaneng.2017.01.014>
- Amrutha MM, Sanil Kumar V, Sharma S, et al (2015) Characteristics of shallow water waves off the central west coast of India before, during and after the onset of the Indian summer monsoon. *Ocean Eng*. 107, 259–270. <https://doi.org/10.1016/j.oceaneng.2015.07.061>
- Amrutha MM, Sanil Kumar V, Bhaskaran H, Naseef TM (2019) Consistency of wave power at a location in the coastal waters of central eastern Arabian Sea. *Ocean Dynamics* 69, 543–560. doi :10.1007/s10236-019-01267-1
- Anoop TR, Kumar VS, Shanas PR, Johnson G (2015) Surface wave climatology and its variability in the north Indian Ocean Based on ERA-interim reanalysis. *J Atmos Ocean Technol*. 32,1372–1385. <https://doi.org/10.1175/JTECH-D-14-00212.1>
- Chen TC, Tsay JD, Matsumoto J, Alpert J (2017) Impact of the summer monsoon westerlies on the South China Sea tropical cyclone genesis in may. *Weather Forecast*. 32(3),925–947.<https://doi.org/10.1175/WAF-D-16-0189.1>
- Chen X, Li C, Li X (2020) Influences of ENSO on boreal summer intraseasonal oscillation over the western Pacific in decaying summer. *Clim Dyn* 54:3461–3473. <https://doi.org/10.1007/s00382-020-05183-9>
- Chu PC, Qi Y, Chen Y, et al. (2004) South China Sea wind-wave characteristics. Part 1: Validation of wavematch-III using TOPEX/Poseidon data. *J Atmos Ocean Technol*. 21(11), 1718–1733. <https://doi.org/10.1175/JTECH1661.1>
- Duchon CE (1979) LANCZOS FILTERING IN ONE AND TWO DIMENSIONS. *J Appl Meteorol*.18(8), 1016–1022. [https://doi.org/10.1175/1520-0450\(1979\)018<1016:LFIOAT>2.0.CO;2](https://doi.org/10.1175/1520-0450(1979)018<1016:LFIOAT>2.0.CO;2)
- Glejin J, Kumar VS, Nair TMB (2013) Monsoon and cyclone induced wave climate over the near shore waters off Puduchery, south western Bay of Bengal. *Ocean Eng* 72:277–286. <https://doi.org/10.1016/j.oceaneng.2013.07.013>

- Godoi VA, de Andrade FM, Bryan KR, Gorman RM (2019) Regional-scale ocean wave variability associated with El Niño–Southern Oscillation–Madden-Julian Oscillation combined activity. 39,483– 494. *Int J Climatol*. <https://doi.org/10.1002/joc.5823>
- Godoi VA, de Andrade FM, Durrant TH, Torres Júnior AR (2020) What happens to the ocean surface gravity waves when ENSO and MJO phases combine during the extended boreal winter? *Clim Dyn*. 54, 1407–1424. <https://doi.org/10.1007/s00382-019-05065-9>
- Grimm AM, Ambrizzi T (2009) Teleconnections into South America from the Tropics and Extratropics on Interannual and Intraseasonal Timescales 14,159-191. https://doi.org/10.1007/978-90-481-2672-9_7
- Han S, Fan Y, Dong Y. et al. (2017) A study on the relationships between the wave height and the El Niño in the north area of the South China Sea. *Acta Oceanol. Sin.* 36, 44–50. <https://doi.org/10.1007/s13131-017-1059-2>
- Hersbach H, Bell B, Berrisford P, et al (2020) The ERA5 global reanalysis. *Q J R Meteorol Soc.* 146,1999– 2049. <https://doi.org/10.1002/qj.3803>
- Hsu P, LeeJ,Ha K, Tsou C (2017) Influences of Boreal Summer Intraseasonal Oscillation on Heat Waves in Monsoon Asia. *Journal of Climate*. 30(18): 7191-7211. <https://doi.org/10.1175/JCLI-D-16-0505.1>
- Jiang H, Chen G (2013) A global view on the swell and wind sea climate by the Jason-1 mission: A revisit. *J Atmos Ocean Technol.* 30(8),1833–1841 <https://doi.org/10.1175/JTECH-D-12-00180.1>
- Jiang X, Li T, Wang B (2004) Structures and mechanisms of the northward propagating boreal summer intraseasonal oscillation. *J Clim*.17(5),1022–1039. [https://doi.org/10.1175/1520-0442\(2004\)017<1022:SAMOTN>2.0.CO;2](https://doi.org/10.1175/1520-0442(2004)017<1022:SAMOTN>2.0.CO;2)
- Kikuchi K, Wang B, Kajikawa Y (2012) Bimodal representation of the tropical intraseasonal oscillation. *Clim Dyn*. 38,1989–2000. <https://doi.org/10.1007/s00382-011-1159-1>
- Klein SA, Soden BJ, Lau NC (1999) Remote sea surface temperature variations during ENSO: Evidence for a tropical atmospheric bridge. *J Clim*. 12(4), 917–932. [https://doi.org/10.1175/1520-0442\(1999\)012<0917:RSSTVD>2.0.CO;2](https://doi.org/10.1175/1520-0442(1999)012<0917:RSSTVD>2.0.CO;2)
- Krishnamurti TN, Subrahmanyam D (1982) The 30-50 day mode at 850 mb during MONEX. *J Atmos Sci*.39(9), 2088–2095. [https://doi.org/10.1175/1520-0469\(1982\)039<2088:TDMAMD>2.0.CO;2](https://doi.org/10.1175/1520-0469(1982)039<2088:TDMAMD>2.0.CO;2)
- Kumar VS, Kumar KA, Anand NM (2000) Characteristics of waves off Goa, West coast of India, *Journal of Coastal Research* 16(3), 782-789. www.jstor.org/stable/4300088
- Kumar P, Kaur S, Weller E, Min SK (2019) Influence of Natural Climate Variability on the Extreme Ocean Surface Wave Heights Over the Indian Ocean. *J Geophys Res Ocean.*_124, 6176– 6199. <https://doi.org/10.1029/2019JC015391>
- Kumar P, Min SK, Weller E, et al (2016) Influence of climate variability on extreme ocean surface wave heights assessed from ERA-interim and ERA-20C. *J Clim* 29:4031–4046. <https://doi.org/10.1175/JCLI-D-15-0580.1>

- Li Chong-Yin, Zhou Ya-Ping (1994) Relationship between intraseasonal oscillation in the tropical atmosphere and ENSO. *Chinese Journal Geophysics*.37. 17-26
- Li J, Mao J (2019) Factors controlling the interannual variation of 30–60-day boreal summer intraseasonal oscillation over the Asian summer monsoon region. *Clim Dyn* 52:1651–1672. <https://doi.org/10.1007/s00382-018-4216-1>
- Li XM (2016) A new insight from space into swell propagation and crossing in the global oceans. *Geophys Res Lett* 43:5202–5209. <https://doi.org/10.1002/2016GL068702>
- Lin H (2019) Long-lead ENSO control of the boreal summer intraseasonal oscillation in the East Asian-western North Pacific region. *npj Clim Atmos Sci* 2:1–6. <https://doi.org/10.1038/s41612-019-0088-2>
- Lin H, Derome J, Brunet G (2007) The nonlinear transient atmospheric response to tropical forcing. *J Clim* 20:5642–5665. <https://doi.org/10.1175/2007JCLI1383.1>
- Liu F, Li T, Wang H, et al (2016) Modulation of boreal summer intraseasonal oscillations over the Western North Pacific by ENSO. *J Clim* 29:7189–7201. <https://doi.org/10.1175/JCLI-D-15-0831.1>
- Madden RA, Julian PR (1972) Description of Global-Scale Circulation Cells in the Tropics with a 40–50 Day Period. *J Atmos Sci*.29(6), 1109–1123. [https://doi.org/10.1175/1520-0469\(1972\)029<1109:dogsc>2.0.co;2](https://doi.org/10.1175/1520-0469(1972)029<1109:dogsc>2.0.co;2)
- Mirzaei A, Tangang F, Juneng L, et al (2013) Wave climate simulation for southern region of the South China Sea. *Ocean Dyn* 63:961–977. <https://doi.org/10.1007/s10236-013-0640-2>
- Naseef TM, Sanil Kumar V (2020) Climatology and trends of the Indian Ocean surface waves based on 39-year long ERA5 reanalysis data. *Int J Climatol.* 40, 979-1006, <https://doi.org/10.1002/joc.6251>
- Odériz I, Silva R, Mortlock TR, Mori N (2020) ENSO Impacts on Global Wave Climate and Potential Coastal Hazards. *J Geophys Res Ocean.* 125, e2020JC016464. <https://doi.org/10.1029/2020jc016464>
- Patra A, Min S, Seong M (2020) Climate Variability Impacts on Global Extreme Wave Heights: Seasonal Assessment Using Satellite Data and ERA5 Reanalysis. *J Geophys Res Ocean.* 125, e2020JC016754. <https://doi.org/10.1029/2020jc016754>
- Pillai PA, Chowdary JS (2016) Indian summer monsoon intra-seasonal oscillation associated with the developing and decaying phase of El Niño. *Int J Climatol.* 36,1846-1862. <https://doi.org/10.1002/joc.4464>
- Praveen PGRB, Srinivas KG, Nair TMB (2020) Impact of tropical and extra tropical climate variability on Indian Ocean surface waves. *Clim Dyn* 54:4919–4933. <https://doi.org/10.1007/s00382-020-05262-x>
- Ramon J, Lledó L, Torralba V, et al (2019) What global reanalysis best represents near-surface winds? *Q J R Meteorol Soc* 145, 3236–3251. <https://doi.org/10.1002/qj.3616>

- Rasmusson EM, Carpenter TH (1982) Variations in tropical sea surface temperature and surface wind fields associated with the Southern Oscillation/ El Nino (Pacific). *Mon Weather Rev.* 110, 354–384. [https://doi.org/10.1175/1520-0493\(1982\)110<0354:VITSST>2.0.CO;2](https://doi.org/10.1175/1520-0493(1982)110<0354:VITSST>2.0.CO;2)
- Remya PG, Kumar BP, Srinivas G, Nair TMB (2020) Impact of tropical and extra tropical climate variability on Indian Ocean surface waves. *Clim Dyn* 54:4919–4933. <https://doi.org/10.1007/s00382-020-05262-x>
- Sabique L, Annapurnaiah K, Balakrishnan Nair TM, Srinivas K (2012) Contribution of Southern Indian Ocean swells on the wave heights in the Northern Indian Ocean - A modeling study. *Ocean Eng* 43:113–120. <https://doi.org/10.1016/j.oceaneng.2011.12.024>
- Sanil Kumar V, Anoop TR (2015) Wave energy resource assessment for the Indian shelf seas. *Renew Energy*. 76, 212-219, <https://doi.org/10.1016/j.renene.2014.11.034>
- Sanil Kumar V, George J (2016) Influence of Indian summer monsoon variability on the surface waves in the coastal regions of eastern Arabian Sea. *Ann Geophys* 34:871–885. <https://doi.org/10.5194/angeo-34-871-2016>
- Schott, F. A., Xie, S.-P., McCreary, J.P (2009) Indian Ocean circulation and climate variability, *Rev. Geophys.*, 47, RG1002, doi:10.1029/2007RG000245.
- Shanas PR, Kumar VS (2015) Trends in surface wind speed and significant wave height as revealed by ERA-Interim wind wave hindcast in the Central Bay of Bengal. *Int J Climatol*. 35, 2654–2663, <https://doi.org/10.1002/joc.4164>
- Shanas PR, Aboobacker VM, Albarakati MA, Zubier KM (2017) Climate driven variability of wind-waves in the Red Sea, *Ocean Modelling* 119, 105-117, <https://doi.org/10.1016/j.ocemod.2017.10.001>
- Shimura T, Mori N, Mase H (2015) Future projection of ocean wave climate: Analysis of SST impacts on wave climate changes in the Western North Pacific. *J Clim.* 28, 3171–3190. <https://doi.org/10.1175/JCLI-D-14-00187.1>
- Srinivas G, Remya PG, Malavika S, Nair TMB (2020) The influence of boreal summer intra-seasonal oscillations on Indo-western Pacific Ocean surface waves. *Sci Rep* 10, 1–12. <https://doi.org/10.1038/s41598-020-69496-9>
- Su H, Wei C, Jiang S, et al (2017) Revisiting the seasonal wave height variability in the South China Sea with merged satellite altimetry observations. *Acta Oceanol Sin.* 36, 38–50. <https://doi.org/10.1007/s13131-017-1073-4>
- Yasunari T (1979) Cloudiness Fluctuations Associated with the Northern Hemisphere Summer Monsoon. *J Meteorol Soc Japan Ser II.* 57, 227-242. https://doi.org/10.2151/jmsj1965.57.3_227
- Yun KS, Seo KH, Ha KJ (2008) Relationship between ENSO and northward propagating intraseasonal oscillation in the east Asian summer monsoon system. *J Geophys Res Atmos.* 113, D14120. <https://doi.org/10.1029/2008JD009901>
- Zheng CW, Li CY, Pan J (2018) Propagation Route and Speed of Swell in the Indian Ocean. *J Geophys Res Ocean* 123, 8– 21. <https://doi.org/10.1002/2016JC012585>

Table 1. Number of days under each combination of ENSO – BSISO phases for the period 1979-2018 over the season JJAS

BSISO Phase	ENSO - Neutral	El Niño	La Niña
1	111	68	27
2	89	64	24
3	104	76	48
4	126	74	58
5	113	68	32
6	105	75	30
7	115	78	39
8	129	84	53

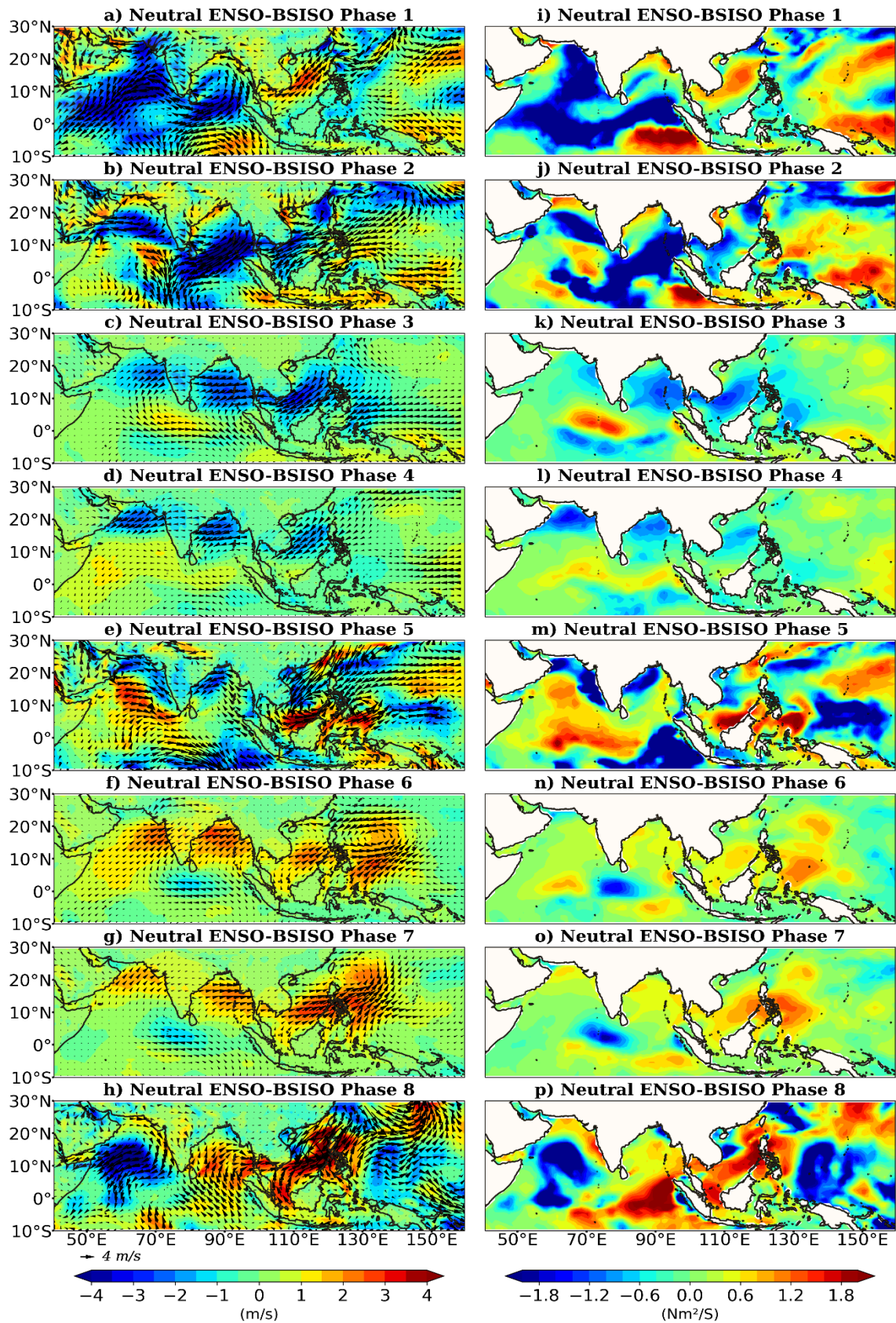


Fig. 1 Daily anomaly composites of 10 m wind (left column) and energy flux from the wind into the waves (right column) for Neutral ENSO - BSISO combined phase over JJAS season during the period 1979-2018

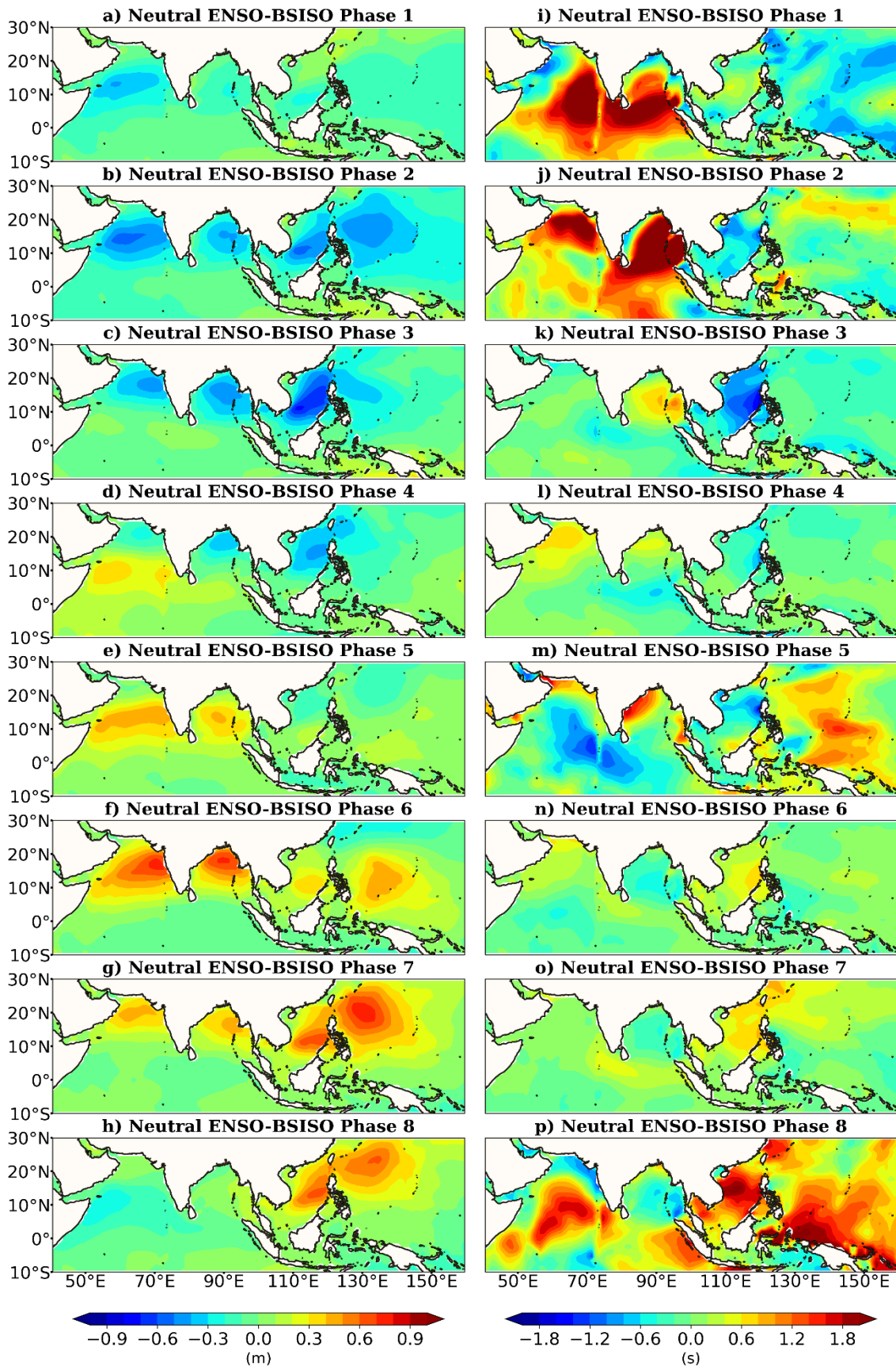


Fig. 2 Daily anomaly composites of significant wave height (left column) and mean wave period (right column) for Neutral ENSO - BSISO combined phase over JJAS season during the period 1979-2018

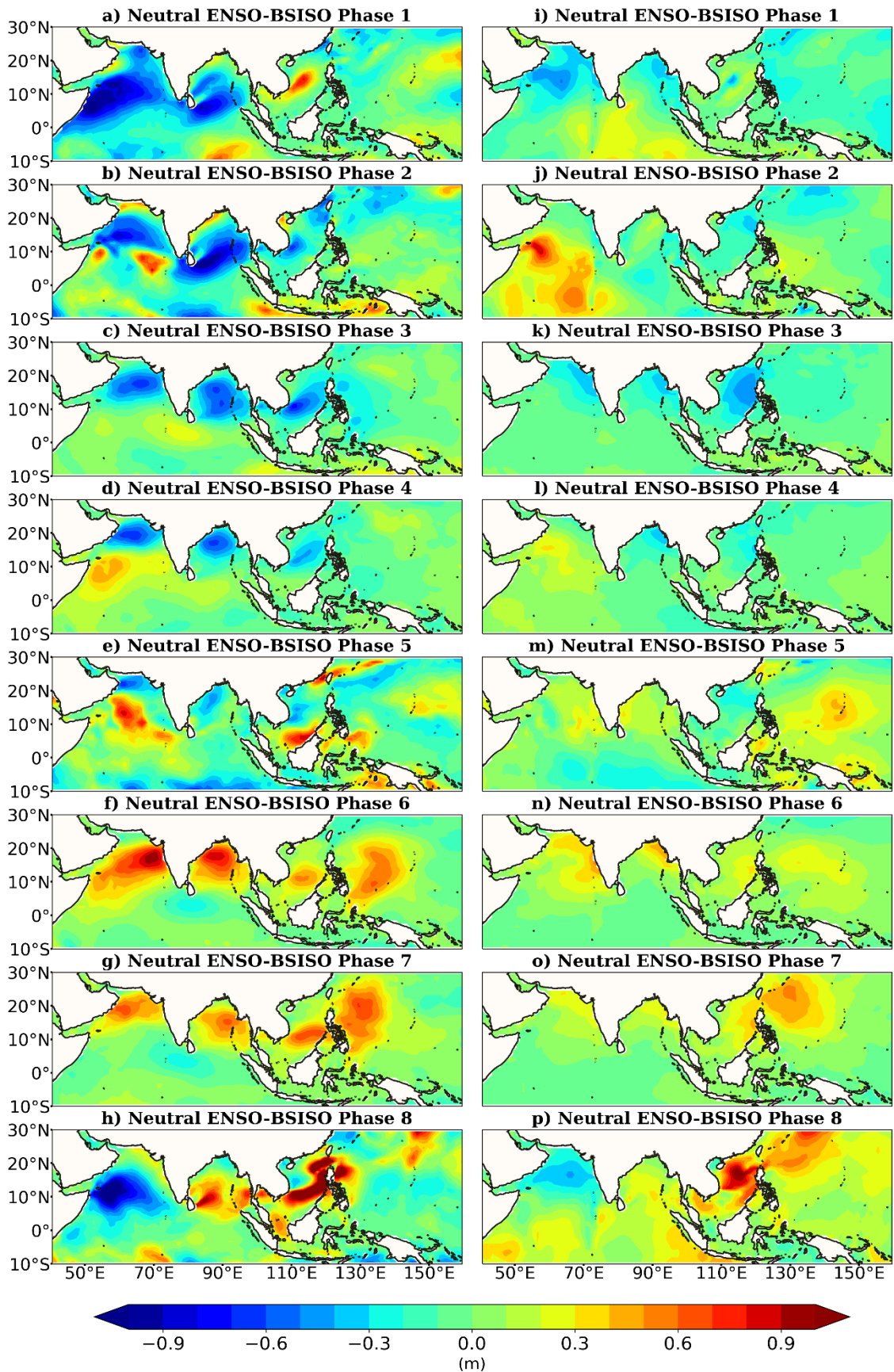


Fig. 3 Daily anomaly composites of significant height of wind-seas (left column) and significant height of swells (right column) for Neutral ENSO - BSISO combined phase over JJAS season during the period 1979-2018

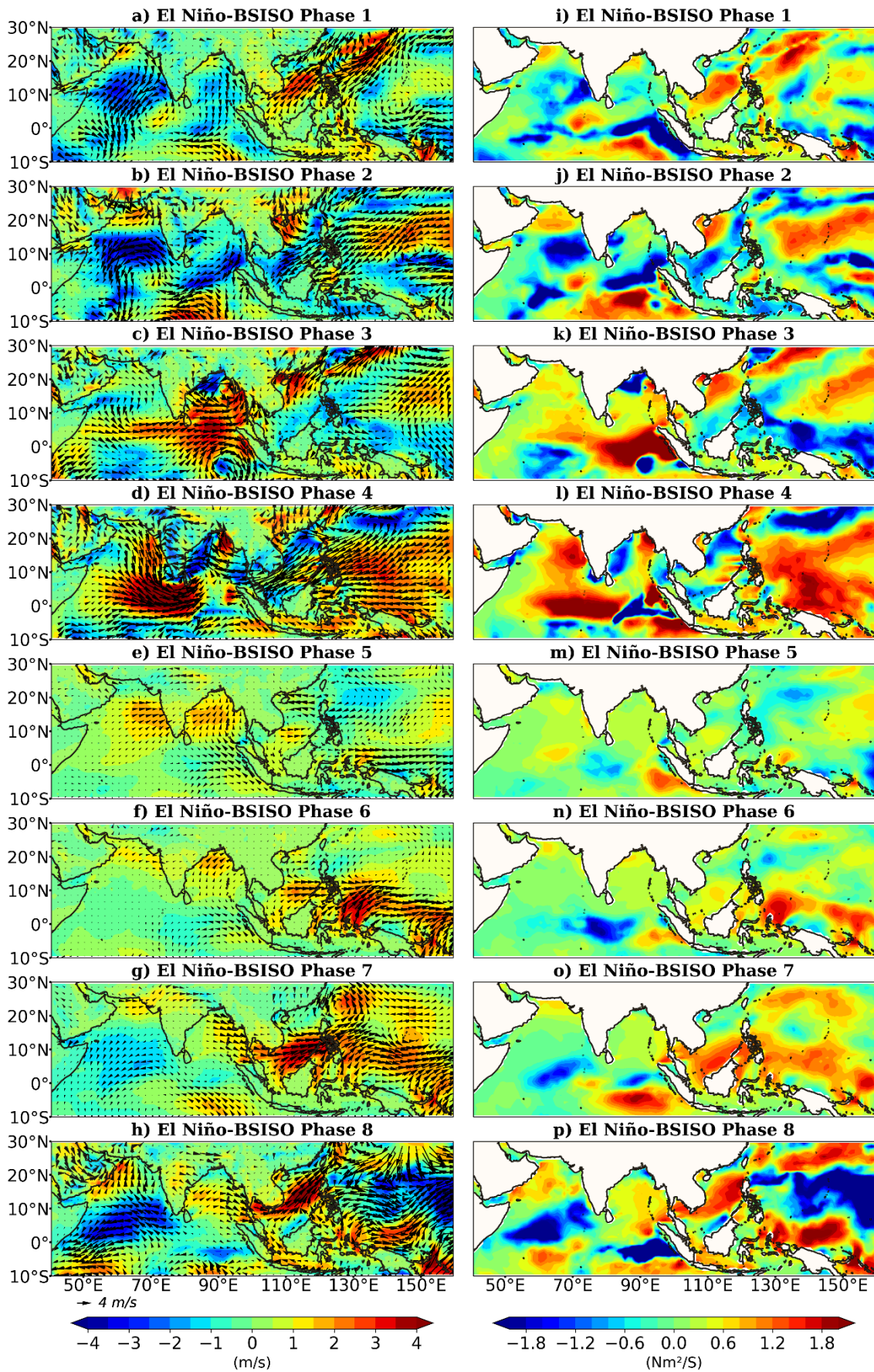


Fig. 4 Daily anomaly composites of 10 m wind (left column) and vertical energy flux into the waves (right column) for El Niño - BSISO combined phase over JJAS season during the period 1979-2018

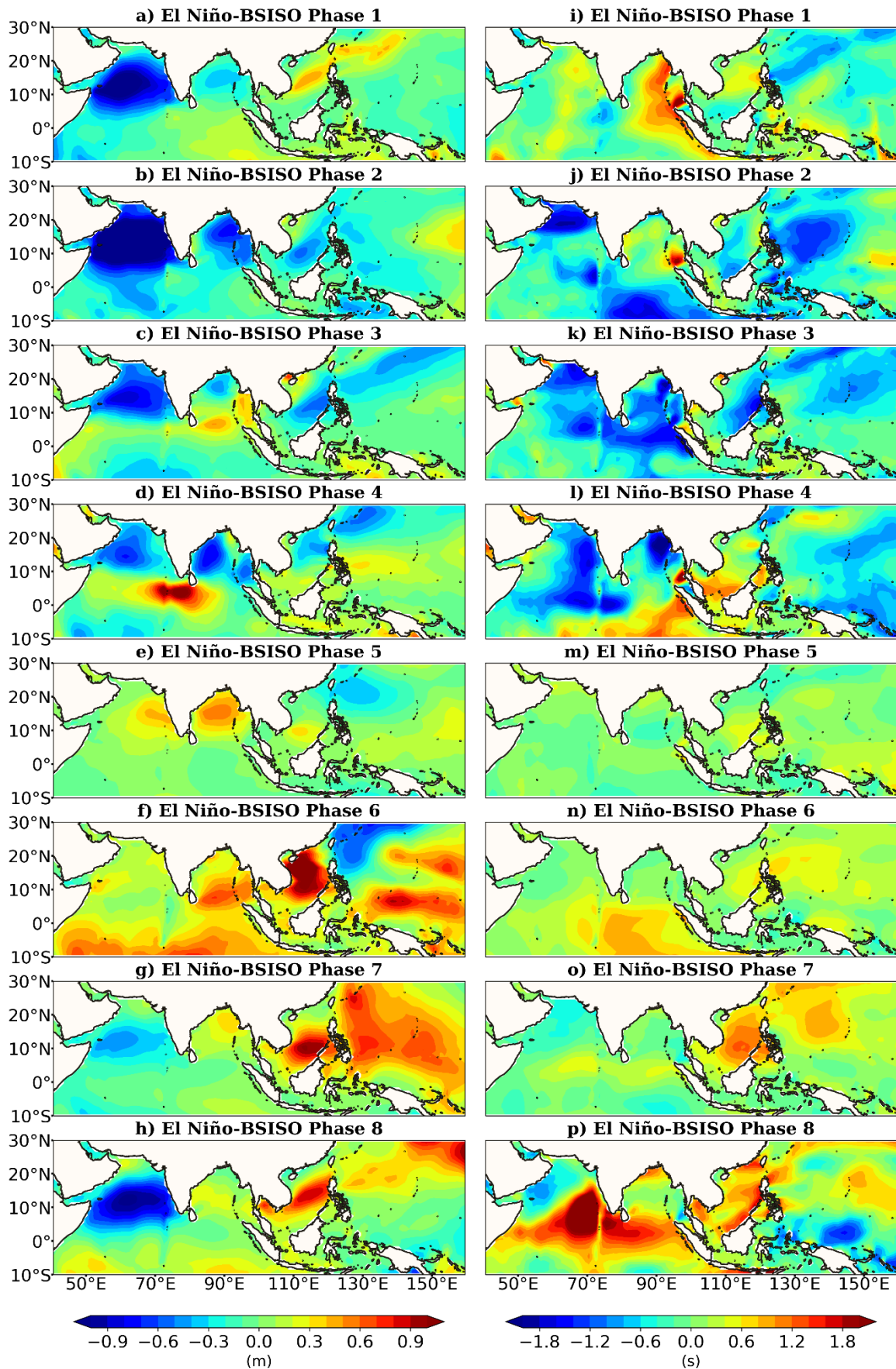


Fig. 5 Daily anomaly composites of significant wave height (left column) and mean wave period (right column) for El Niño - BSISO combined phase over JJAS season during the period 1979-2018

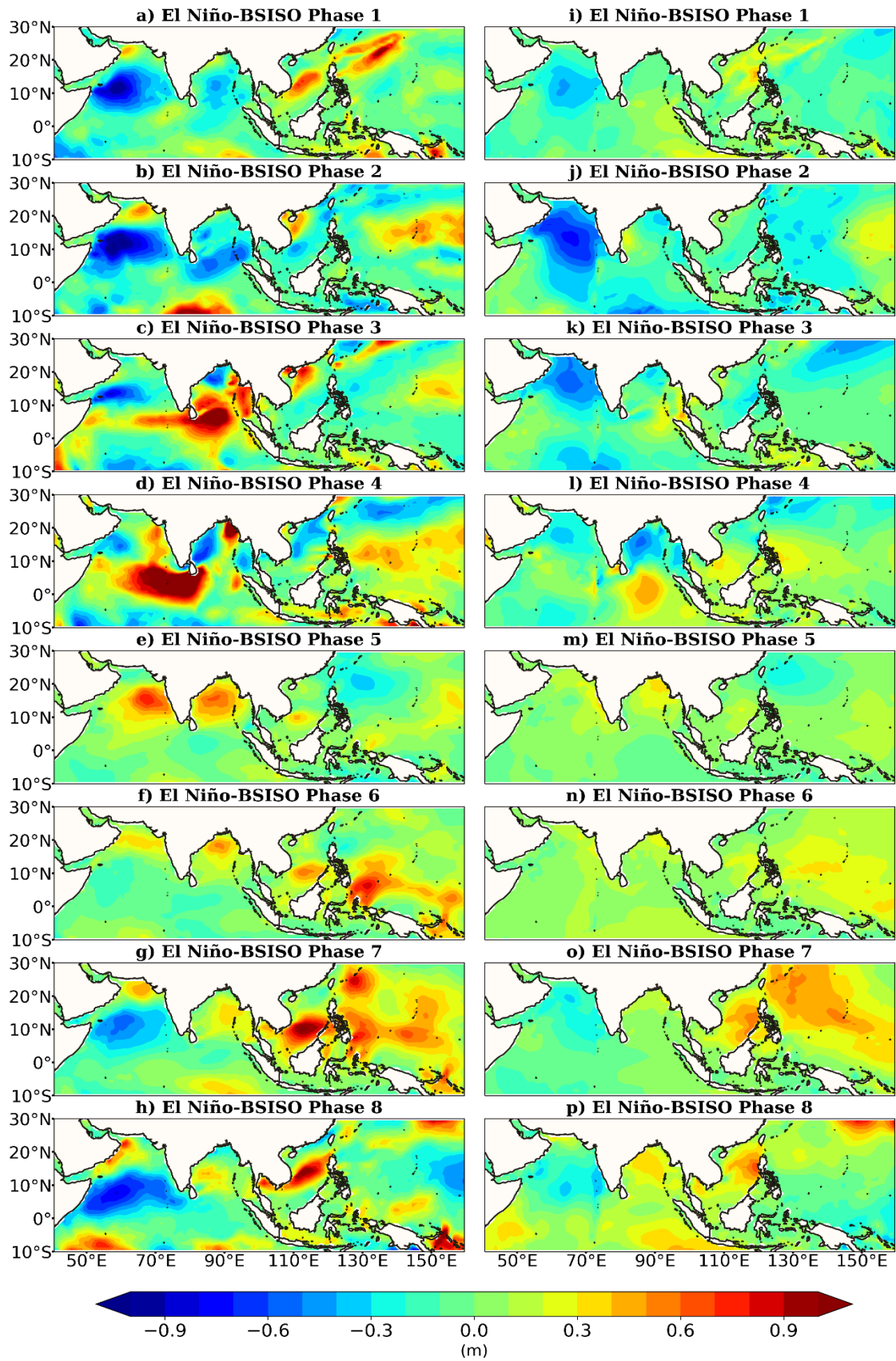


Fig. 6 Daily anomaly composites of significant height of wind-seas (left column) and significant height of swells (right column) for El Niño - BSISO combined phase over JJAS season during the period 1979-2018

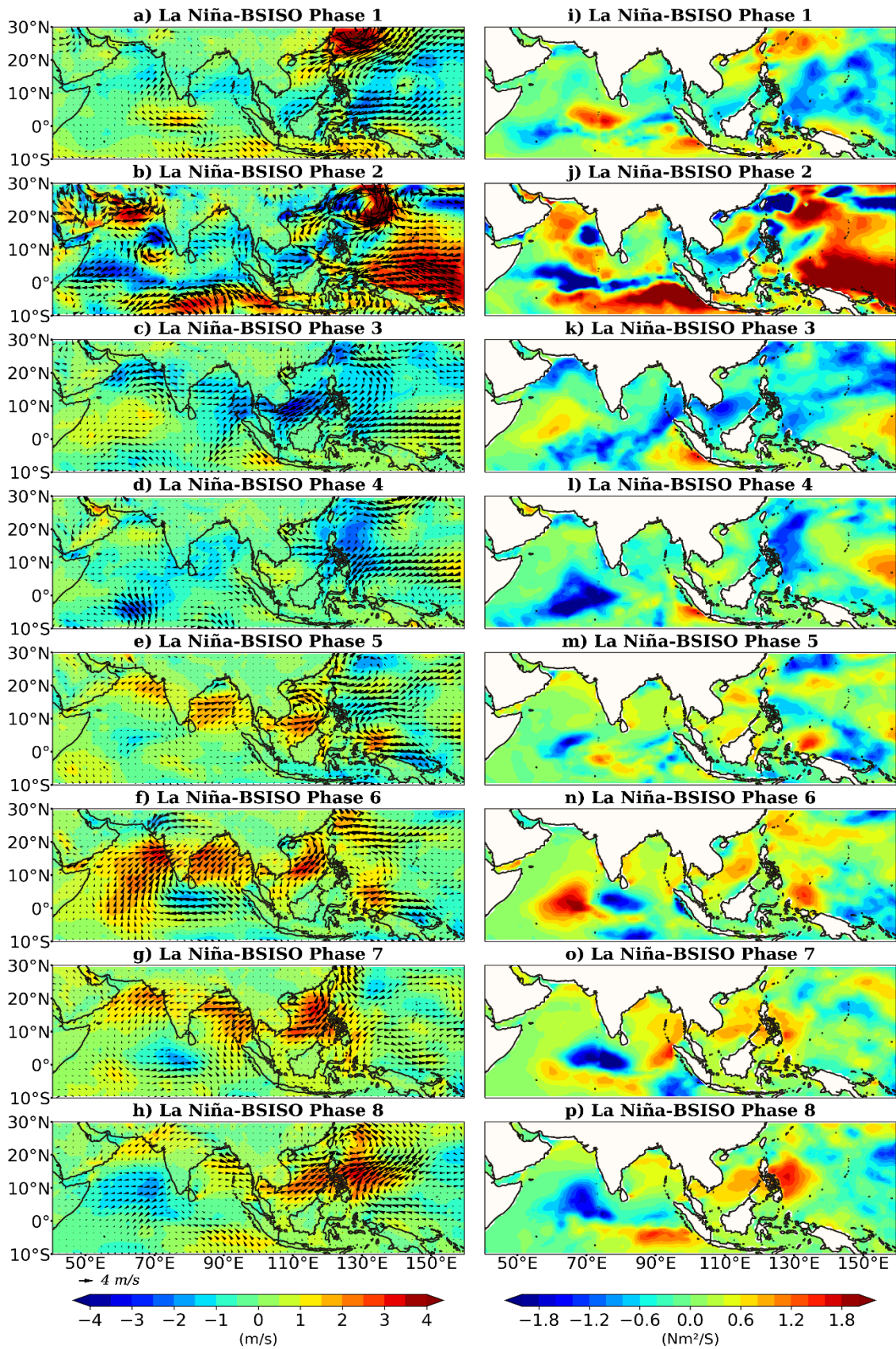


Fig. 7 Daily anomaly composites of 10 m wind (left column) and energy flux from the wind into the waves (right column) for La Niña - BSISO combined phase over JJAS season during the period 1979-2018

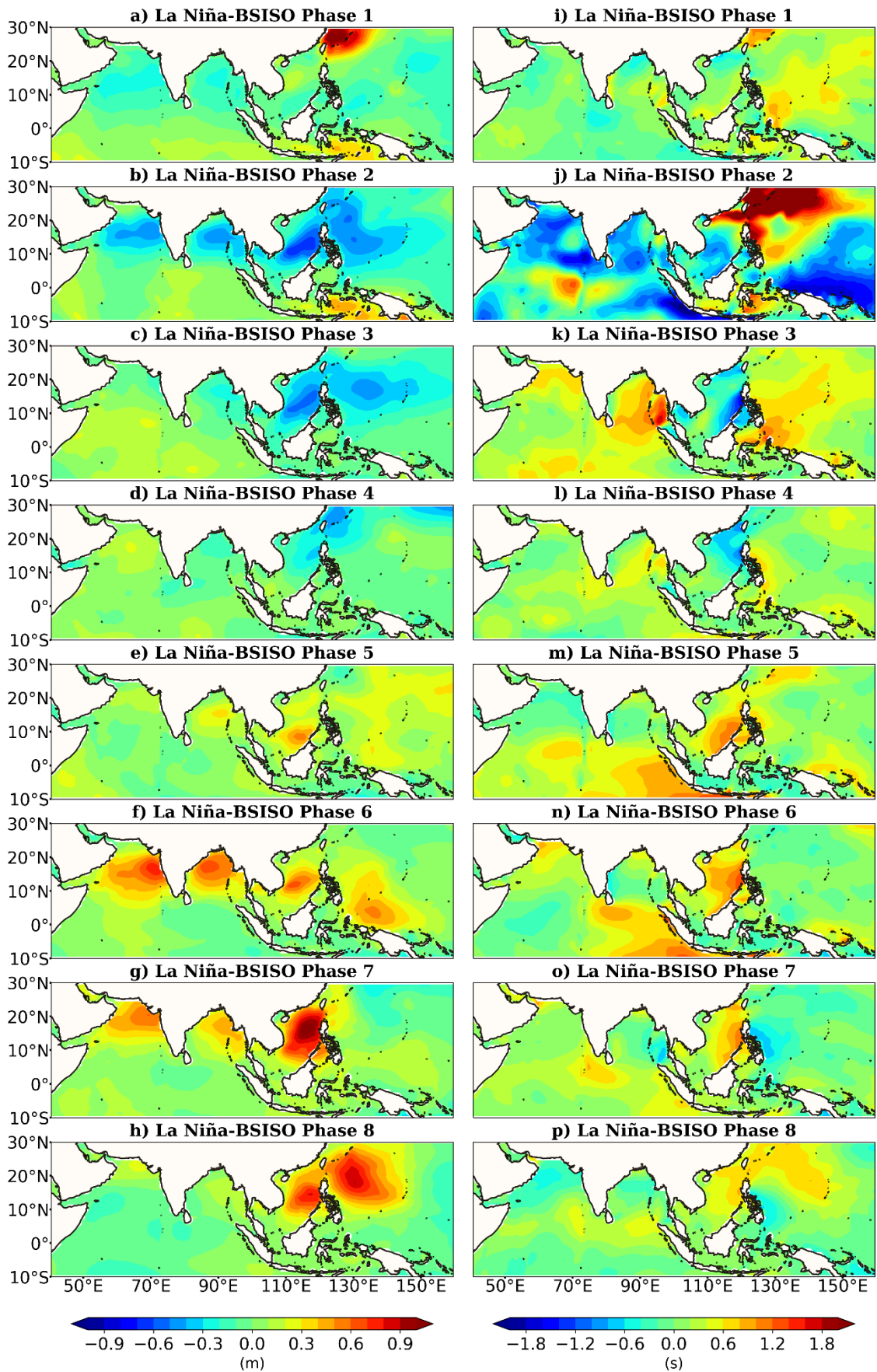


Fig. 8 Daily anomaly composites of significant wave height (left column) and mean wave period (right column) for La Niña - BSISO combined phase over JJAS season during the period 1979-2018

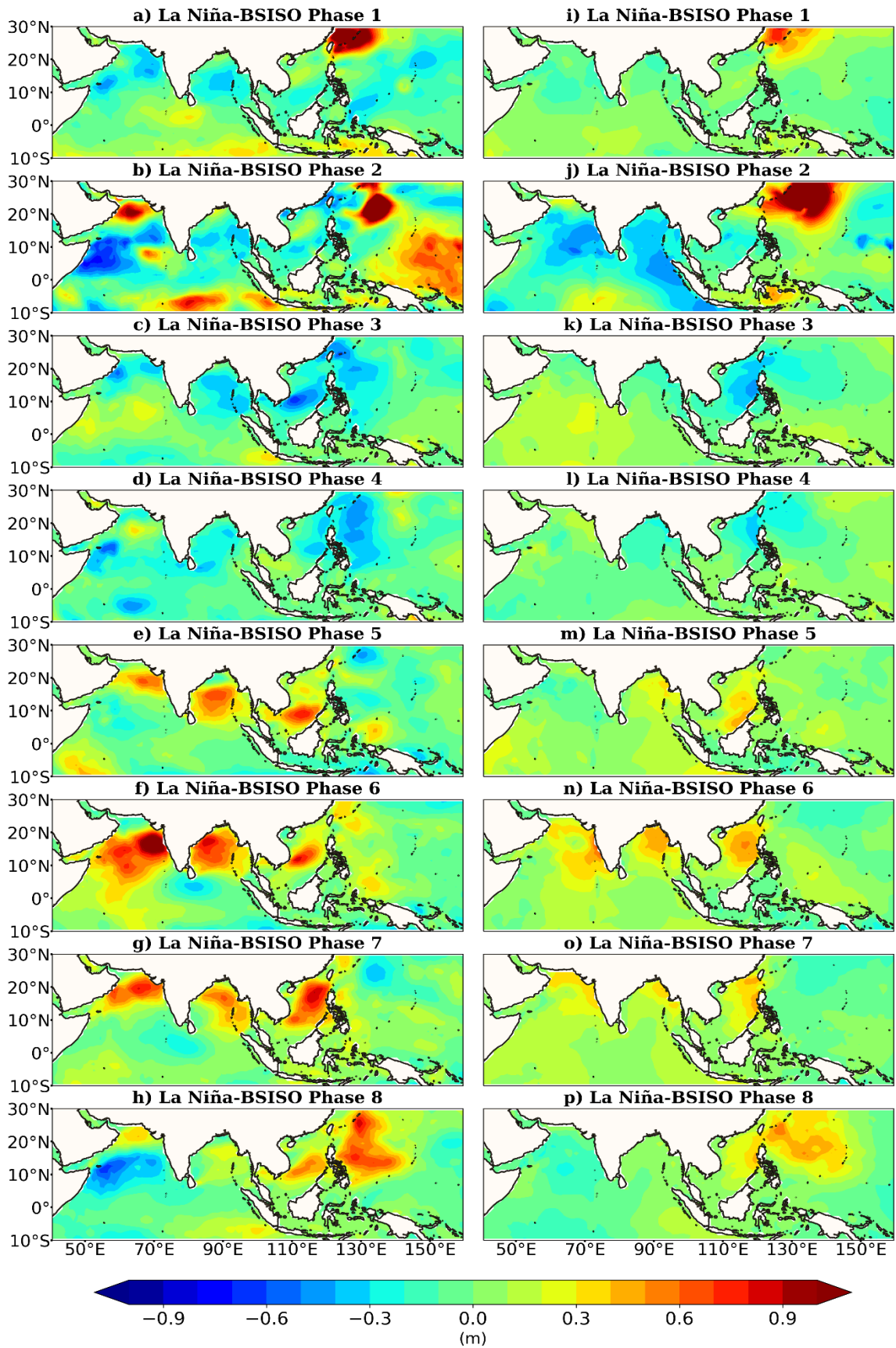


Fig. 9 Daily anomaly composites of significant height of wind-seas (left column) and significant height of swells (right column) for La Niña - BSISO combined phase over JJAS season during the period 1979-2018